ACS APPLIED MATERIALS & INTERFACES

Research Article

www.acsami.org

Defect-Induced Loss Mechanisms in Polymer–Inorganic Planar Heterojunction Solar Cells

Michael Hartel,[†] Song Chen,[†] Benjamin Swerdlow,[†] Hsien-Yi Hsu,[‡] Jesse Manders,[†] Kirk Schanze,[‡] and Franky So*,[†]

[†]Department of Materials Science and Engineering and [‡]Department of Chemistry, University of Florida, Gainesville, Florida 32611, United States

ABSTRACT: The effect of ZnO defects on photoexcited charge carrier recombination and forward induced charge transfer was studied in organic–inorganic bilayer organic heterojunction solar cells. Decreased bimolecular recombination via passivation of ZnO nanopariticle defects resulted in longer carrier lifetime as determined by transient photovoltage (TPV) measurements. It was also found by time-resolved photoluminescence (TRPL) measurements that defect passivation decreased the fluorescence lifetime which indicated higher exciton dissociation efficiency. Through passivation of the ZnO nanoparticles defects, the two loss mechanisms were reduced and the power conversion efficiency (PCE) is significantly enhanced.

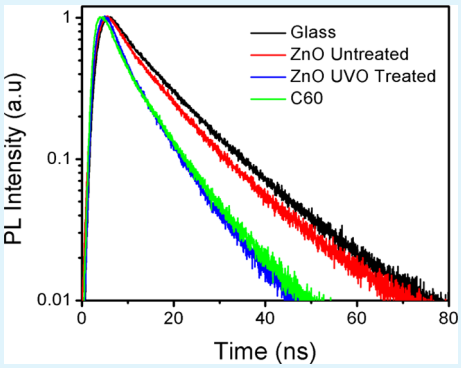

KEYWORDS: *organic solar cell, ZnO nanoparticles, PCDTBT, defects, transient photovoltage, PL lifetime*

Progress in the field of organic photovoltaics (OPVs) is rapid due to the synthesis of new materials and development of new device architectures.[1−3] For roll-to-roll processing, inverted structure is desired and metal oxides such as ZnO have been used as the electron transporting layer for inverted OPV devices.[4−6] Additionally, there is a drive to use metal oxides as an acceptor due to their high dielectric constant (ε = 10)[7] compared to organic acceptors such as C_{60} (ε = 4).[8] The higher dielectric constant facilitates exciton dissociation by reducing the Coulombic attraction of the bound electron–hole pair. ZnO has also been used as an electron acceptor in various device structures.[9−11] However, the efficiency in these hybrid cells utilizing ZnO nanorods as the acceptor is lower than 1%.[12] Recently, UV-ozone (UVO) treatment of the ZnO nanoparticles (NPs) charge collection contact was shown to improve the device performance in inverted, low bandgap polymer/fullerene bulk heterojunction solar cells.[6] However, the effect of ZnO defects on exciton dissociation and charge recombination at the donor/acceptor interface have not been studied in detail.

In this work, donor–acceptor copolymer/ZnO NPs bilayer heterojunction devices were fabricated. The effect of subbandgap defects in ZnO NPs films on device performance was studied and two photocurrent loss mechanisms were identified. Transient photovoltage measurements (TPV) showed reduced interface recombination of photogenerated carriers in devices with UVO treatment. Also, time-resolved photoluminescence (TRPL) measurements indicate increased photoinduced charge transfer after defect passivation by UVO treatment. Therefore, the population of ZnO defects plays an important role in the device performance.

ZnO NPs were synthesized according to the method previously reported[13−15] and have diameters of 5 nm.[6] The synthesis was performed by dropwise addition of a stoichiometric amount of tetramethylammonium hydroxide dissolved in ethanol (0.55 M) to 30 mL of 0.1 M zinc acetate dehydrate dissolved in dimethyl sulfoxide (DMSO) under continuous stirring. After precipitation and dispersion in ethanol, 35 nm ZnO NPs films were formed by spincasting followed by a 100 °C heat treatment in air. In order to passivate the ZnO defects, a 5 min UVO treatment, optimized for solar cell performance, was carried out on the ZnO NPs films using a UVLS-225D UV lamp (50 W). In order to verify the passivation of ZnO defects, photoluminescence (PL) measurements were performed. Figure 1 shows the effect of UVO treatment on the PL spectra. The band edge in the absorption matches the 360 nm excitonic peak shown in the PL spectra. The strong broad-band peak centered at 515 nm has been attributed to emission due to subgap defects.[16−20] Before the treatment, the ratio of the intensity of the excitonic peak to that of the defect peak was 1:0.6. After the treatment, the ratio is significantly reduced to 1:0.2 due to the reduction of oxygen vacancies and surface dangling bonds present.[16]

In order to understand the nature of the ZnO defects, X-ray photoemission spectroscopy (XPS) was carried out. Figure 2a and b shows the O1s region of the XPS spectra of the as-prepared and UVO treated films, respectively. The lower

Received: April 26, 2013
Accepted: July 11, 2013
Published: July 11, 2013

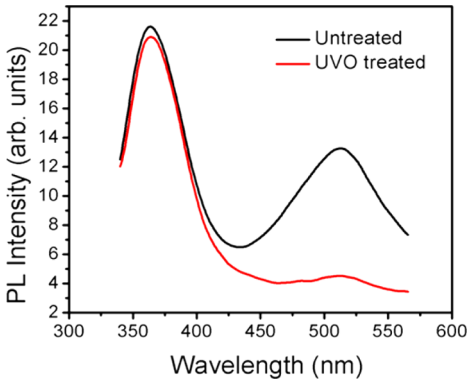

Figure 1. Steady state PL spectra of ZnO NP films. The band edge emission is located at 365 nm while the defect emission is between 425 and 575 nm.

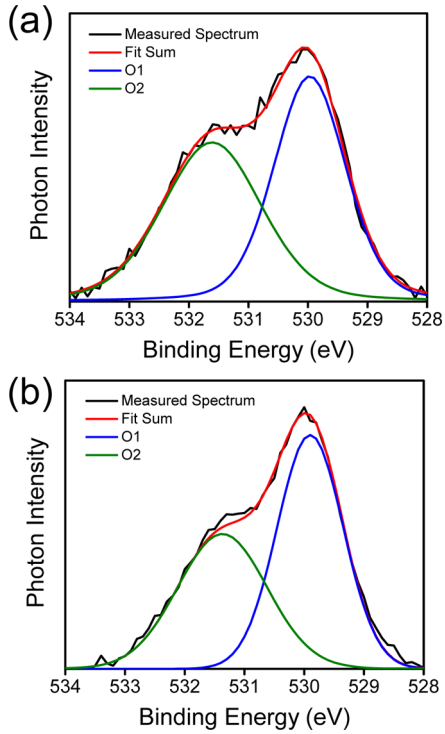

Figure 2. XPS spectra O1s peak for (a) untreated ZnO NP and (b) treated ZnO NP films. The data is split into two Gaussian peaks. The lower binding energy peak at 530 eV is attributed to O_2^- ions present in a stoichiometric wurtzite ZnO structure, whereas the higher binding energy peak at 531.5 eV is associated with O_2^- ions in oxygen-deficient regions of the ZnO matrix.

binding energy peak at 530 eV (O1) in both figures is attributed to O_2^- ions present in a stoichiometric wurtzite ZnO structure, whereas the higher binding energy peak at 531.5 eV (O_2) is associated with O_2^- ions in oxygen-deficient regions of the ZnO matrix.[21] Before UVO treatment, the ratio of peak area of O1 to O2 shown in the figures is 1:1.39. After treatment, the peak area ratio changes to 1:1.04, indicating that UVO treatment reduces the concentration of oxygen vacancies and hence the midgap defect states in the ZnO NPs.

To further study the effect of UVO treatment on the ZnO NPs surface, atomic force microscopy (AFM) images were taken in tapping mode. Figure 3a and b shows the height images of a ZnO NP film before and after UVO treatment,

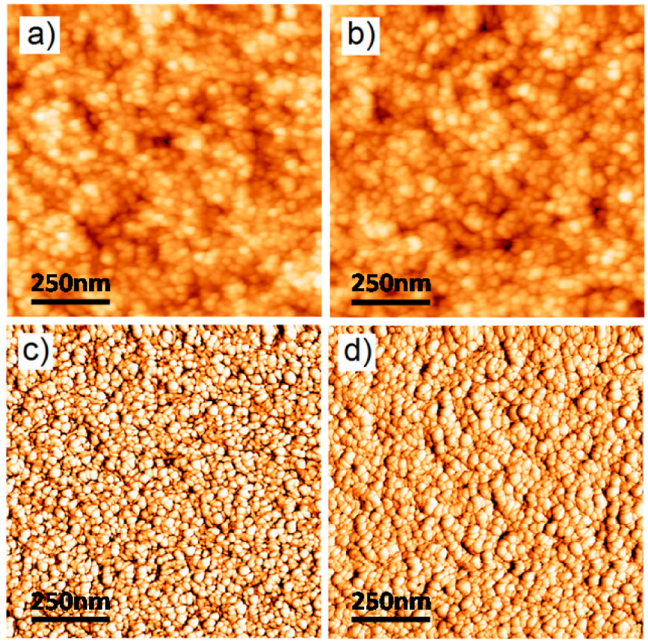

Figure 3. AFM images of untreated ZnO NP film surface (a,c) and UVO treated surface (b,d). Images a and b are height images, while c and d are phase images.

respectfully. The root mean squared (RMS) roughness of both films is ~4.1 nm, indicating that there is no change in film morphology upon UVO treatment. Figures 3c and d show the phase images of the untreated and treated ZnO NP films, respectfully. With UVO treatment, the phase roughness RMS decreases from 6.6° to 4.8°, indicating that the UVO treatment leads to changes in the surface chemistry of the film.

OPV devices were fabricated employing both UVO treated and untreated films. Devices were fabricated on pre-patterned ITO-coated glass substrates with a sheet resistance of 20 Ω/sq. The substrates were cleaned in the following sequence: ultrasonication in acetone, isopropanol, and deionized water for 15 min each, followed by a rinsing in deionized water. The ZnO NP films were spin-cast from a solution using chloroform as the solvent and dried at 100 °C in air yielding a thickness of 35 nm. A UVO treatment of 5 min was then carried out. A 75 nm film of poly[*N*-9′-hepta-decanyl-2,7-carbazole-alt-5,5-(4′,7′-di-2-thienyl-2′,1′,3′-benzothiadiazole)] (PCDTBT) was spin-cast from a solution using chlorobenzene as the solvent and annealed at 70 °C for 30 min in a nitrogen glovebox. The anode was thermally evaporated and consisted of a 5 nm thick layer of MoOx and a 100 nm thick layer of Ag.

The current density−voltage (J−V) characteristics of the devices measured under a 100 mW cm^{-2} AM 1.5G solar simulator are shown in Figure 4a. The active area of each device was 4.6 mm^2. Devices with and without UVO treatment had the same open-circuit voltage (V_{OC}) of 0.70 V indicating no change in the energy level offset between the conduction band of ZnO NPs and the highest occupied molecular orbital (HOMO) of PCDTBT. There is however, a significant improvement in short-circuit current (J_{sc}) and fill factor when the ZnO NPs film is UVO treated. The device without UVO treatment has a J_{sc} of 0.60 mA cm^{-2} and a fill factor (FF) of 0.39 yielding a power conversion efficiency (PCE) of 0.19%. The devices employing UVO treated ZnO NPs layers have a J_{SC} of 1.30 mA cm^{-2} and FF of 0.55, yielding a PCE of 0.52%

dx.doi.org/10.1021/am4015605 | ACS Appl. Mater. Interfaces 2013, 5, 7215−7218

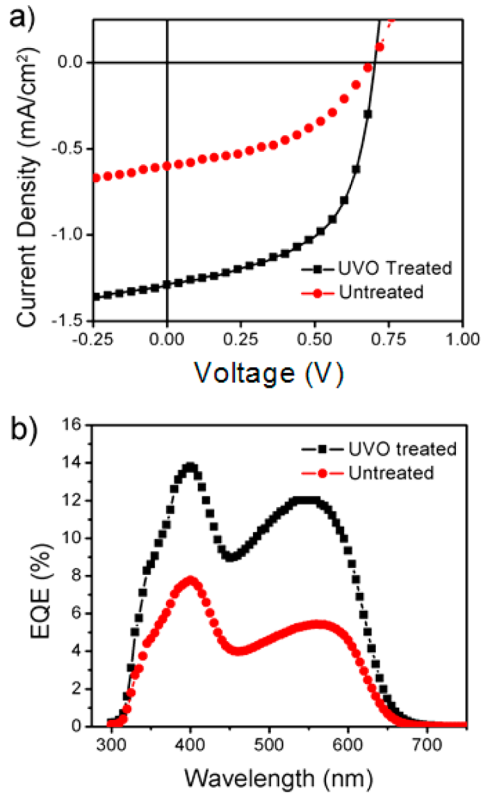

Figure 4. (a) J–V characteristics and (b) EQE spectra of PCDTBT/ZnO cells. The devices with and without UVO treatment are plotted with squares and triangles, respectively.

which is more than a 2.5× enhancement compared to the untreated device. The average results from eight devices are summarized in Table I. The external quantum efficiency (EQE) spectra measured for the PCDTBT/ZnO devices are shown in Figure 4b. For the device employing UVO treated ZnO NPs films, the EQE reaches 13.7% compared to just 7.8% for the device with untreated ZnO NPs. Bilayer devices were also fabricated using poly[2-methoxy-5-(3′,7′-dimethyloctyloxy)-1,4-phenylenevinylene]) (MDMO-PPV) as the donor polymer. For MDMO-PPV/ZnO devices fabricated on untreated ZnO NPs films, the J_{sc} and FF were 0.35 mA cm^{-2} and 41%, respectively. Devices employing the UVO treated film showed an improved J_{sc} and FF of 0.76 mA cm^{-2} and 46%, respectively, leading to a PCE increase from 0.12% to 0.28%. Our device data, along with the PL data in Figure 1, suggest that defect passivation in ZnO NPs due to UVO treatment leads to reduction in carrier recombination and enhancement in forward charge transfer, resulting in enhancements in both J_{sc} and fill factor. We also speculate that the UVO treatment effect is not only a surface treatment; the active oxygen can penetrate into the ZnO NPs film and affect the NPs under than top surface. The details of the phenomenon will be studied in our future work.

Table I. Photovoltaic Parameters of PCDTBT/ZnO Hybrid Solar Cells

donor polymer	ZnO treatment	V_{OC} (V)	J_{sc} (mA cm^{-2})	FF (%)	PCE (%)
PCDTBT	none	0.70	0.60 ± 0.03	39 ± 1	0.19 ± 0.02
PCDTBT	5 min UVO	0.70	1.30 ± 0.04	55 ± 2	0.52 ± 0.02
MDMO-PPV	none	0.83	0.35 ± 0.03	41 ± 1	0.12 ± 0.03
MDMO-PPV	5 min UVO	0.77	0.76 ± 0.02	46 ± 2	0.26 ± 0.02

To study the effect of defect passivation on carrier recombination, transient photovoltage (TPV) measurements were done on devices with and without UVO treatment and the results are plotted in Figure 5. In a bilayer structured polymer/ZnO solar cell, bulk recombination is dominated by bimolecular processes that occur at the polymer/ZnO interface. Thus, the defect density could directly impact the interface recombination rate of the solar cell. Any differences in carrier lifetime can therefore be attributed to defects on the surface of ZnO. The TPV setup used in this study has been previously described.[22] For this measurement, the devices were photo-biased using a 100 mW cm^{-2} AM 1.5G white light. A voltage perturbation (25 mV) was generated by a 527 nm optical pulse with a width of 8 ns. This low level excitation allows the photovoltage decay to follow a single exponential behavior through which the carrier lifetime can be extracted (Figure. 5). The carrier lifetime (τ) measured for devices with the UVO treated ZnO NPs films was found to be 365 ns compared to only 186 ns for devices with untreated ZnO. Since the TPV measurements were done under open-circuit condition, our data indicate the recombination at the PCDTBT/ZnO interface at zero field is one of the mechanisms of loss mechanism, resulting in a low fill factor for the untreated device. Defect passivation due to UVO treatment leads to an enhancement of fill factor from 39% to 55% for PCDTBT devices and from 41% to 46% in MDMO-PPV devices.

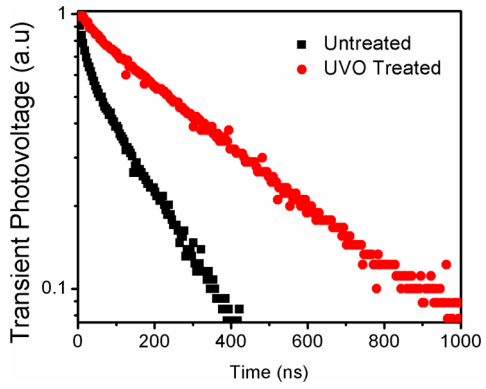

Figure 5. Transient photovoltage decay for devices employing untreated (black squares) and UVO treated (red circles).

To study the forward charge transfer from the polymer to ZnO NPs, TRPL measurements were performed with a time-correlated single photon counting (TCSPC) spectrometer (Picoquant, Inc.). A pulsed laser (375 nm) with an average power of 1 mW, operating at 40 MHz, with duration of 70 ps was used to excite the PCDTBT film. It should be noted that the excitation is not absorbed by ZnO NPs and the fluorescence signal comes from the polymer only. Figure 6 shows the 700 nm PCDTBT fluorescence decay of a PCDTBT/ZnO bilayer film sample. PL decays of 25 nm thick PCDTBT films on a bare glass substrate, as processed ZnO NP film, and a UVO treated ZnO NPs film were also measured for comparison. To compare ZnO NPs as an electron acceptor with the commonly used fullerene in polymer solar cells, TRPL measurements were also done on a PCDTBT film

dx.doi.org/10.1021/am4015605 | ACS Appl. Mater. Interfaces 2013, 5, 7215–7218

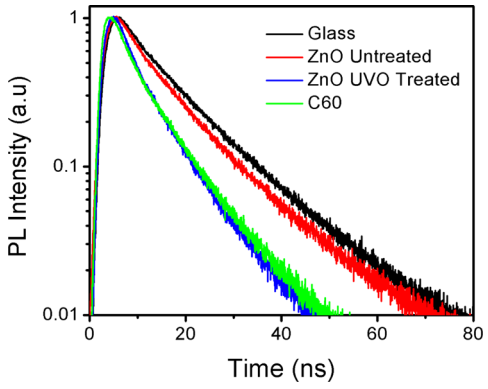

Figure 6. Fluorescence lifetime curves of 10 nm films of PCDTBT on various surfaces. The PL signal at 700 nm was monitored after excitation at 375 nm.

deposited on a thermally evaporated C_{60} film. Here, C_{60} was used because thermally evaporated C_{60} does not mix with PCDTBT after spin coating. By fitting the decay curves, the measured PL lifetimes for PCDTBT on the glass substrate, as-processed ZnO, UVO-treated ZnO, and C_{60} are determined to be 1.39, 1.24, 0.80, and 0.88 ns, respectively.[10] Upon UVO treatment of ZnO NPs, it is expected that passivation of ZnO defects leads to an enhancement in separation of photogenerated electron–hole pairs and, hence, a reduction in fluorescence lifetime. Therefore, a shorter PL lifetime indicates a more efficient charge transfer for devices employing a UVO-treated ZnO NPs film. With UVO treatment, the ZnO NPs film even surpasses fullerene for exciton dissociation. These results are expected since the dielectric constant of ZnO (ε = 10) is higher than the fullerene (ε = 4) while the conduction band offset at the PCDTBT/ZnO junction is sufficiently large for electron transfer. Here, the enhanced charge separation has led to an enhancement of J_{sc} from 0.6 to 1.3 mA cm^{-2} in PCDTBT/ZnO devices.

In summary, we report two defect-induced loss mechanisms in polymer/ZnO planar heterojunction solar cells. By passivation of defects at the PCDTBT/ZnO interface, devices showed enhancements in the short-circuit current and fill factor resulting in a power conversion efficiency improvement of over 250% compared to the devices using untreated films. Transient photovoltage measurements showed that the passivation to ZnO defects leads to a reduction of interface recombination of photocarriers and hence an improvement in fill factor. Time-resolved fluorescence measurements showed a shorter PL lifetime upon UVO treatment of ZnO indicating more efficient forward photoinduced charge transfer and an enhancement in short-circuit current. This work shows that defects in ZnO are the culprit for low power conversion efficiencies in these hybrid solar cells and defect passivation is important to significantly improve the device performance.

AUTHOR INFORMATION

Corresponding Author

*E-mail: fso@mse.ufl.edu.

Notes

The authors declare no competing financial interest.

ACKNOWLEDGMENTS

We acknowledge the support of the Department of Energy Basic Energy Sciences (contract no.: DE-FG0207ER46464) for this work.

REFERENCES

(1) Po, R.; Maggini, M.; Camaioni, N. *J. Phys. Chem. C* **2010**, *114*, 695.
(2) Xue, J. G. *Polym. Rev.* **2010**, *50*, 411.
(3) Chen, L. M.; Hong, Z. R.; Li, G.; Yang, Y. *Adv. Mater.* **2009**, *21*, 1434.
(4) Amb, C. M.; Chen, S.; Graham, K. R.; Subbiah, J.; Small, C. E.; So, F.; Reynolds, J. R. *J. Am. Chem. Soc.* **2011**, *133*, 10062.
(5) Kyaw, A. K. K.; Sun, X. W.; Jiang, C. Y.; Lo, G. Q.; Zhao, D. W.; Kwong, D. L. *Appl. Phys. Lett.* **2008**, *93*, No. 221107.
(6) Chen, S.; Small, C. E.; Amb, C. M.; Subbiah, J.; Lai, T. H.; Tsang, S. W.; Manders, J. R.; Reynolds, J. R.; So, F. *Adv. Energy Mater.* **2012**, *2*, 1333.
(7) Langton, N. H.; Matthews, D. *Br. J. Appl. Phys.* **1958**, *9*, 453.
(8) Ching, W. Y.; Huang, M.-Z.; Xu, Y.-N.; Harter, W. G.; Chan, F. T. *Phys. Rev. Lett.* **1991**, *67*, 2045.
(9) Olson, D. C.; Lee, Y. J.; White, M. S.; Kopidakis, N.; Shaheen, S. E.; Ginley, D. S.; Voigt, J. A.; Hsu, J. W. P. *J. Phys. Chem. C* **2008**, *112*, 9544.
(10) Park, I.; Lim, Y.; Noh, S.; Lee, D.; Meister, M.; Amsden, J. J.; Laquai, F.; Lee, C.; Yoon, D. Y. *Org. Electron.* **2011**, *12*, 424.
(11) Beek, W. J. E.; Wienk, M. M.; Janssen, R. A. J. *Adv. Mater.* **2004**, *16*, 1009.
(12) Baeten, L.; Conings, B.; Boyen, H. G.; D'Haen, J.; Hardy, A.; D'Olieslaeger, M.; Manca, J. V.; Van Bael, M. K. *Adv. Mater.* **2011**, *23*, 2802.
(13) Bera, D.; Qian, L.; Sabui, S.; Santra, S.; Holloway, P. H. *Opt. Mater.* **2008**, *30*, 1233.
(14) Qian, L.; Zheng, Y.; Choudhury, K. R.; Bera, D.; So, F.; Xue, J. G.; Holloway, P. H. *Nano Today* **2010**, *5*, 384.
(15) Qian, L.; Zheng, Y.; Xue, J. G.; Holloway, P. H. *Nat. Photon.* **2011**, *5*, 543.
(16) Leiter, F. H.; Alves, H. R.; Hofstaetter, A.; Hofmann, D. M.; Meyer, B. K. *Phys. Status Solidi B.* **2001**, *226*, R4.
(17) Yang, R. D.; Tripathy, S.; Li, Y. T.; Sue, H. J. *Chem. Phys. Lett.* **2005**, *411*, 150.
(18) Xu, W. L.; Zheng, M. J.; Ding, G. Q.; Shen, W. Z. *Chem. Phys. Lett.* **2005**, *411*, 37.
(19) Xiong, G.; Pal, U.; Serrano, J. G. *J. Appl. Phys.* **2007**, 101.
(20) Vanheusden, K.; Warren, W. L.; Seager, C. H.; Tallant, D. R.; Voigt, J. A.; Gnade, B. E. *J. Appl. Phys.* **1996**, *79*, 7983.
(21) Hsieh, P. T.; Chen, Y. C.; Kao, K. S.; Wang, C. M. *Appl. Phys. A–Mater. Sci. Process.* **2008**, *90*, 317.
(22) Chen, S.; Choudhury, K. R.; Subbiah, J.; Amb, C. M.; Reynolds, J. R.; So, F. *Adv. Energy Mater.* **2011**, *1*, 963.